STU
FCHPT

Quantum-chemical studies of triangulo cobalt-hydride clusters with trimethylphosphine and carbonyl ligands

Martin Breza

Department of Physical Chemistry, Faculty of Chemical and Food Technology STU, Radlinskeho 9, SK-81237 Bratislava, Slovakia
martin.breza@stuba.sk

Abstract: Geometry of neutral $[H_n\{Co(\mu_2\text{-}CO)(PMe_3)_2\}_3]$ complexes, n = 0→4, in three lowest spin states was optimized at the B3LYP/6-311G* level of theory with GD3 dispersion correction. The most stable quartet spin state was found for $[\{Co(\mu_2\text{-}CO)(PMe_3)_2\}_3]$ whereas the doublet or triplet spin states are the most stable in the remaining complexes. Hydrogenation of $[\{Co(\mu_2\text{-}CO)(PMe_3)_2\}_3]$ to the complexes with μ_3-H bridges is more advantageous at lower temperatures. Trigonal symmetry is preserved only in $[(\mu_3\text{-}H)\{Co(\mu_2\text{-}CO)(PMe_3)_2\}_3]$. Neutral H_2 units in $[(H_2)\{Co(\mu_2\text{-}CO)(PMe_3)_2\}_3]$, $[(H_2)(\mu_3\text{-}H)\{Co(\mu_2\text{-}CO)(PMe_3)_2\}_3]$, and $[(H_2)_2\{Co(\mu_2\text{-}CO)(PMe_3)_2\}_3]$ are only physisorbed and show vanishing spin density. Spin density is concentrated dominantly at positively charged Co atoms and only the vanishing spin density is located at the negatively charged μ_3-H atoms. There are no Co—Co bonds and the Co_3 triangles are held together only by μ_2-CO and μ_3-H bridges.

Keywords: DFT calculations; electronic structure; geometry optimization; QTAIM.

Introduction

Atomic clusters exhibit unique structural and electronic characteristics which offer significant potential to achieve novel material properties and functions (Tsukamoto, 2024). Unlike nanoparticles, their small size is the source of eccentric physical and chemical properties implied by quantum effects. Their electronic states resemble rather those of molecules than those of bulk materials. The steric and electronic structures of atomic clusters offer potential for achieving novel properties and functions.

A re-established concern in catalysis by low-valent transition metal clusters is implied by their multiple binding sites and unusual bridging coordination (Hogarth et al., 2010; Böhme and Schwarz, 2010). Moreover, they act as electron buffer for catalytic reactions and can have desirable magnetic properties (Nombel et al., 1999; Moberg et al., 2006; Liu et al., 2015; Craig and Murrie, 2015). Metal carbonyl clusters $[Et_4N]_2[Fe_3(CO)_9E]$ (E = S, Se, Te) were investigated as well (Guzman-Jimenez et al., 2003). The first tricobalt clusters $Co_3(CO)_3(CO)_3L_3$, L = PPh_3 or P^nBu_3 were synthesized in 1969 (Pregaglia et al., 1969) and their hydride X-ray structure was later reformulated as $HCo_3(CO)_3(CO)_3(PPh_3)_3$ (Bradamante et al., 1983). Concurrently, an analogous hydrido cluster $HCo_3(CO)_9$ has been synthesized as deduced by mass spectrometry (Facchinetti et al., 1979, 1981).

Klein et al. (1992a) synthesized the X-ray structure of $[H\{Co(\mu_2\text{-}CO)(PMe_3)_2\}_3]$ by photochemical activation and published. Position of the central μ_3-H atom in the trigonal space group R-3c was deduced based on semiempirical INDO calculations. This compound was used as a catalyst in linear trimerization of phenylethyne (Klein et al., 1992b). The synthesis, X-ray structures, and magnetic properties of a whole series of isostructural triangulo cobalt-hydride clusters $[X\{Co(\mu_2\text{-}CO)(PMe_3)_2\}_3]$, X = none, H, and H_3 (see Fig. 1 and Tab. 1) were published as well (Klein et al., 1997; Boča et al., 2000). $[H_3\{Co(\mu_2\text{-}CO)(PMe_3)_2\}_3]$ was obtained from $[H\{Co(\mu_2\text{-}CO)(PMe_3)_2\}_3]$ and H_2 at 20 °C in tetrahydrofuran.

Paramagnetic $[\{Co(\mu_2\text{-}CO)(PMe_3)_2\}_3]$ complex in doublet spin state (Fig. 1) forms dark violet hexagonal crystals sparingly soluble in toluene, benzene, or tetrahydrofuran (Klein et al., 1997; Boča et al., 2000). Mass spectra indicate the presence of more than 10 % of $[H\{Co(\mu_2\text{-}CO)(PMe_3)_2\}_3]$ in solid $[\{Co(\mu_2\text{-}CO)(PMe_3)_2\}_3]$. The effective magnetic moment slowly decreases (from 1.9 μ_B at room temperature) up to 30 K (1.7 μ_B) and then rapidly drops (1.3 μ_B at 4 K). This can be explained by thermally inaccessible quartet spin state and weak antiferromagnetic interactions between neighboring complexes.

Paramagnetic $[H\{Co(\mu_2\text{-}CO)(PMe_3)_2\}_3]$ complex (in triplet ground spin state) forms a continuous range of mixed crystals with $[\{Co(\mu_2\text{-}CO)(PMe_3)_2\}_3]$ and cannot be separated by recrystallization (Klein et al., 1997; Boča et al., 2000). In the presence of protic acids or metal hydrides, $[H\{Co(\mu_2\text{-}CO)(PMe_3)_2\}_3]$ is

readily transformed to $[H_3\{Co(\mu_2\text{-}CO)(PMe_3)_2\}_3]$, which indicates hydride character of the μ_3-H atom. The effective magnetic moment of $[H\{Co(\mu_2\text{-}CO)(PMe_3)_2\}_3]$ decreases from 3.1 μ_B at 300 K to 2.5 μ_B at ca 30 K and then rapidly drops to 1.7 μ_B at 4 K. This is consistent with two unpaired electrons per molecule, antiferromagnetic coupling in a Co_3 unit and ferromagnetic Co—H coupling. The decrease under 30 K is explained by zero-field splitting of the triplet spin state and/or the antiferromagnetic intermolecular interaction. A tendency to reach a singlet spin state is also possible.

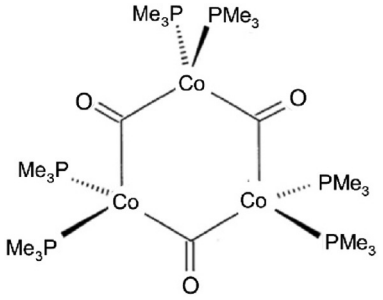

Fig. 1. Schematic structure of $[\{Co(\mu_2\text{-}CO)(PMe_3)_2\}_3]$.

Tab. 1. Interatomic distances (in Å) in X-ray structures of $[H_n\{Co(\mu_2\text{-}CO)(PMe_3)_2\}_3]$ clusters (Klein et al., 1992a; Klein et al., 1997).

n	0	1	3
Co—Co	2.4055(5)	2.421(1)	2.4320(7) 2.4321(7)
Co—H	–	Not detected	1.71(3)
Co—C	1.904(2)	1.921(6) 1.913(10)	1.915(2)
Co—P	2.1929(5)	2.195(2) 2.198(2)	2.202(1)
C—O	1.188(3)	1.172(11)	1.179(4)

$[H_2\{Co(\mu_2\text{-}CO)(PMe_3)_2\}_3]$ was not confirmed by IR spectra (Klein et al., 1997).

Paramagnetic $[H_3\{Co(\mu_2\text{-}CO)(PMe_3)_2\}_3]$ (in triplet ground spin state) can be recrystallized from tetrahydrofuran (Klein et al., 1997; Boča et al., 2000). Mass spectra show successive loss of three H atoms, and IR spectra indicate at least one μ_3-H moiety. However, hydrogenation of cyclopentene or cyclohexene in tetrahydrofuran by this complex failed. The effective magnetic moment of $[H_3\{Co(\mu_2\text{-}CO)(PMe_3)_2\}_3]$ is nearly temperature independent up to 2.6 μ_B at 20 K and then rapidly decreases to 1.59 μ_B at 4 K. The explanation is similar to that for $[H\{Co(\mu_2\text{-}CO)(PMe_3)_2\}_3]$. However, magnetic susceptibility down to 3.8 K confirms antiferromagnetic coupling within the Co_3 ring and Co—H interaction of antiferromagnetic nature.

Semiempirical INDO study (Breza, 1994) of the electronic structure of $^2[\{Co(\mu_2\text{-}CO)(PMe_3)_2\}_3]^0$ and $^3[H\{Co(\mu_2\text{-}CO)(PMe_3)_2\}_3]^0$ in the $[\{Co(\mu_2\text{-}CO)(PMe_3)_2\}_3]^0$ experimental geometry (the left superscript denotes the spin multiplicity while the right superscript denotes the charge of the molecule) indicate positive H charges. Very high electron density is concentrated at the Co_3 ring (negative Co charges). Central μ_3-H atoms are most probably located over the center of the Co_3 triangle (1.2—1.3 Å). Co atoms are held together via carbonyl bridges rather than by direct Co—Co bonding.

The aim of our recent study is a quantum-chemical study of neutral triangulo-$[H_nCo_3(\mu_2\text{-}CO)_3(PMe_3)_6]$ clusters, n = 0→4, in various spin states to explain experimentally observed data. In the first step, structure of the model clusters was optimized. Subsequently, their geometries (especially the positions of added H atoms) and electronic structures were compared. Regarding the size of the clusters under study, standard DFT treatment was used.

Method

Geometry optimization of neutral $[H_n\{Co(\mu_2\text{-}CO)(PMe_3)_2\}_3]$ molecules, n = 0→4, in three lowest spin states was performed using the Gaussian16 software (Frisch et al., 2016) using the B3LYP hybrid functional (Becke, 1993) with GD3 dispersion correction (Grimme et al., 2010). The 6-311G* basis sets from the Gaussian16 library (Frisch et al., 2016) were used for all atoms and the non-methyl hydrogens were augmented with p functions. The optimized structures were tested on the absence of imaginary vibrations to confirm that they correspond to the minima of the adiabatic potential surface. The complexes in singlet spin states (S) were treated using unrestricted formalism within a 'broken symmetry' treatment (BS) and its energy (E_S) was corrected in the relation to the high spin state (HS) as follows:

$$E_S = E_{HS} + (E_{BS} - E_{HS})\frac{< S^2 >_{HS}}{< S^2 >_{HS} - < S^2 >_{BS}} \qquad (1)$$

where E_{HS} and E_{BS} are high-spin (HS) and 'broken symmetry' (BS) energies, respectively, whereas $<S^2>_{HS}$ and $<S^2>_{BS}$ are the corresponding spin-square values (Malrieu and Trinquier, 2012). Quintet spin states were used as the HS ones. Gibbs energy as the sum of DFT energy E and Gibbs energy contribution (G_{contr}) in case of the singlet spin state (G_S) can be approximated as

$$G_S = E_S + G_{contr,BS} \qquad (2)$$

where $G_{contr,BS}$ is Gibbs energy contribution in the BS state (Saito et al., 2009).

Electronic structure of the complexes studied was evaluated in terms of Quantum Theory of Atoms-in-Molecule (QTAIM; Bader 1994). QTAIM topological analysis of electron density is a powerful tool for chemical bonding and structure analysis in molecules and crystals. The first derivative (gradient) of the electron density vanishes at its 'critical points' (CP) such as maxima, minima, and saddle points.

Atom positions are determined by electron density maxima. QTAIM atomic charges are obtained using the electron density integrated over atomic basins.

In equilibrium geometry, a pair of bonded atoms are linked by a line, i.e., a bond path along which the electron density is maximally concentrated (ridges of electron density). The presence of a bond path between two atoms is the necessary (but not sufficient) condition for the presence of a chemical bond. The set of bond paths for a given molecule, the molecular graph, faithfully recovers the network of chemical bonds assigned based on chemical considerations. The saddle point of electron density at the bond path is a bond critical point (BCP).

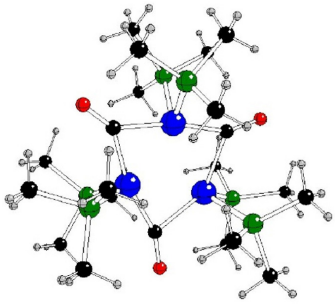

$^{4}[\{Co(\mu_2\text{-}CO)(PMe_3)_2\}_3]^0$
model A

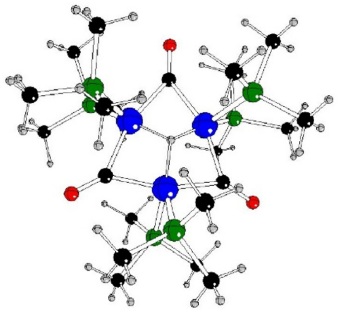

$^{3}[(\mu_3\text{-}H)\{Co(\mu_2\text{-}CO)(PMe_3)_2\}_3]^0$
model B

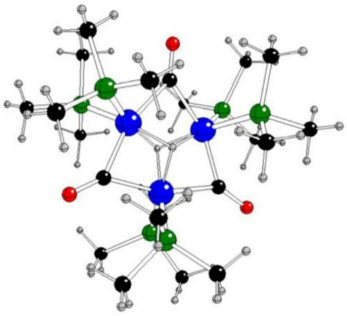

$^{2}[(\mu_3\text{-}H)_2\{(\mu_2\text{-}CO)(PMe_3)_2\}_3]^0$
model C1

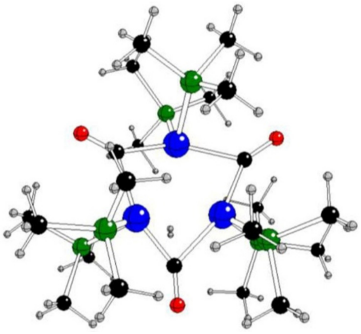

$^{2}[(H_2)\{C_3(\mu_2\text{-}CO)(PMe_3)_2\}_3]^0$
model C2

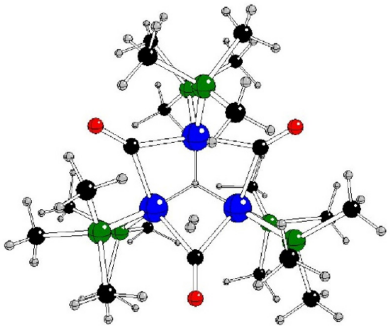

$^{3}[(H_2)(\mu_3\text{-}H)\{Co(\mu_2\text{-}CO)(PMe_3)_2\}_3]^0$
model D

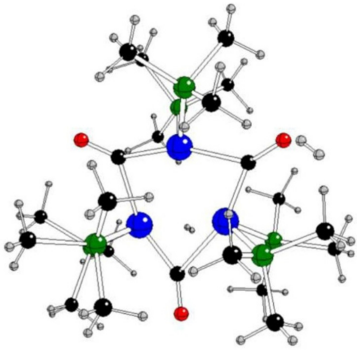

$^{2}[(H_2)_2\{Co(\mu_2\text{-}CO)(PMe_3)_2\}_3]^0$
model E

Fig. 2. Optimized geometries of model systems under study in the most stable spin states (Co – blue, C – black, O – red, P – green, H – gray).

Tab. 2. Absolute DFT energies (E_{DFT}), and Gibbs energies at 298 K (G_{298}), and their relative values related to $^4[\{Co(\mu_2\text{-}CO)(PMe_3)_2\}_3]^0$ (ΔG_{298}), average spin-square values ($<S^2> = S(S+1)$), related spin (S), and relative abundance of individual spin states of the same compound of model systems $[H_n\{Co(\mu_2\text{-}CO)(PMe_3)_2\}_3]$ in various spin states defined by spin multiplicities (M_S). The most stable spin states of individual complexes are denoted in bold.

n	Model	M_S	E_{DFT} [hartree]	G_{298} [hartree]	$<S^2>$	S	ΔG_{298} [kJ/mol]	Relative abundance [%]
0	A	2	–7255.57495	–7254.94365	1.4158	0.7906	7.7	4.3
		4	**–7255.57531**	**–7254.94657**	**3.9475**	**1.5488**	0.0	95.7
		6	–7255.51520	–7254.88980	8.8095	2.5097	149.1	0.0
1	B	1	–7256.18630[a)]	–7255.54623[a)]	1.1239	0.6721	–1603.8[b)]	35.3
		3	**–7256.19928**	**–7255.55797**	**2.1639**	**1.0537**	–1605.3	64.7
		5	–7256.13628	–7255.49964	6.1386	2.0276	–1452.1	0.0
2	C1	**2**	**–7256.77269**	**–7256.12844**	**1.1433**	**0.6804**	–3103.1	100.0
		4	–7256.74928	–7256.10430	3.8154	1.5163	–3039.7	0.0
		6	–7256.70765	–7256.07484	8.9475	2.5327	–2962.4	0.0
	C2	**2**	**–7256.74530**	**–7256.09832**	**1.6532**	**0.8796**	–3024.0	100.0
		4	–7256.73400	–7256.09615	3.9398	1.5469	–3018.3	0.0
		6	–7256.69178	–7256.05110	8.8138	2.5106	–2900.1	0.0
3	D	1	–7257.35707[a)]	–7256.70031[a)]	1.1284	0.6741	–4628.0[b)]	2.6
		3	**–7257.36818**	**–7256.71265**	**2.1743**	**1.0572**	–4637.0	97.4
		5	–7257.31730	–7256.67566	6.1388	2.0276	–4539.9	0.0
4	E	**2**	**–7257.92627**	**–7257.27248**	**1.6506**	**0.8786**	–6106.9	99.9
		4	–7257.92381	–7257.26446	3.9650	1.5530	–6085.9	0.0
		6	–7257.87440	–7257.22477	8.8121	2.5103	–5981.6	0.0

Remarks:

[a)]uncorrected value in the BS state

[b)]corrected value according to Eq. (2).

Tab. 3. Reaction Gibbs energies ($\Delta_r G_T$) of hydrogenation reactions at various temperatures (T).

Reaction	$\Delta_r G_{298}$ [kJ/mol]	$\Delta_r G_{200}$ [kJ/mol]	$\Delta_r G_{100}$ [kJ/mol]
$^4[\{Co(\mu_2\text{-}CO)(PMe_3)_2\}_3]^0 + 0.5\ ^1(H_2)^0 \rightarrow ^3[(\mu_3\text{-}H)\{Co(\mu_2\text{-}CO)(PMe_3)_2\}_3]^0$	–54.9	–64.5	–73.4
$^4[\{Co(\mu_2\text{-}CO)(PMe_3)_2\}_3]^0 + ^1(H_2)^0 \rightarrow ^2[(\mu_3\text{-}H)_2\{Co(\mu_2\text{-}CO)(PMe_3)_2\}_3]^0$	–2.3	–16.3	–29.5
$^4[\{Co(\mu_2\text{-}CO)(PMe_3)_2\}_3]^0 + ^1(H_2)^0 \rightarrow ^2[(H_2)\{Co(\mu_2\text{-}CO)(PMe_3)_2\}_3]^0$	76.8	63.8	51.5
$^4[\{Co(\mu_2\text{-}CO)(PMe_3)_2\}_3]^0 + 1.5\ ^1(H_2)^0 \rightarrow ^3[(H_2)(\mu_3\text{-}H)\{Co(\mu_2\text{-}CO)(PMe_3)_2\}_3]^0$	14.2	–5.3	–23.6
$^4[\{Co(\mu_2\text{-}CO)(PMe_3)_2\}_3]^0 + 2\ ^1(H_2)^0 \rightarrow ^2[(H_2)_2\{Co(\mu_2\text{-}CO)(PMe_3)_2\}_3]^0$	94.8	75.8	54.4

QTAIM bond characteristics are usually evaluated in terms of electron density (ρ), its Laplacian ($\nabla^2\rho$), bond ellipticity (ε), and delocalization indices (DI). The electron density Laplacian ($\nabla^2\rho$) is defined as:

$$\nabla^2\rho = \lambda_1 + \lambda_2 + \lambda_3 \quad (2)$$

and bond ellipticity (ε) is given as:

$$\varepsilon = \frac{\lambda_1}{\lambda_2} - 1 \quad (3)$$

where λ_i are eigenvalues of the Hessian of BCP electron density, $\lambda_1 < \lambda_2 < 0 < \lambda_3$. BCP electron density ($\rho_{BCP}$) is proportional to the bond strength; the value and sign of its BCP Laplacian ($\nabla^2\rho_{BCP}$) describes the relative electron density contribution of bonded atoms to the bond (covalent *vs.* dative bonding); its BCP bond ellipticity (ε_{BCP}) describes its deviation from cylindrical symmetry (such as in ideal single or triple bonds) due to its double-bond character, mechanical strain, and other perturbations.

Electron delocalization index DI(A,B) is the average number of electrons delocalized (shared) between atoms A and B (Keith, 2019). It is used as a bond

Tab. 4. Relevant interatomic distances and bond angles in model systems $[H_n\{Co(\mu_2\text{-}CO)(PMe_3)_2\}_3]$ in the most stable spin states (M_S).

n	0	1	2	2	3	4
Model	A	B	C1	C2	D	E
M_S	4	3	2	2	3	2
Distance [Å]						
Co—Co	2.524 2.489 2.445	2.420(3×)	2.459(2×) 2.381	2.537 2.530 2.568	2.428 2.459 2.430	2.536 2.572 2.529
$Co—C_{C=O}$	1.765, 2.055 1.785, 2.108 1.918, 1.869	1.914(3×) 1.896(3×)	1.912, 1.979 1.890, 1.888 1.981, 1.910	1.814, 2.054 1.818, 2.102 1.802, 2.086	1.893, 1.918 1.909, 1.920 1.904, 1.910	2.116, 1.800 2.078, 1.815 2.045, 1.819
Co—P	2.180, 2.181 2.281, 2.279 2.215, 2.213	2.214(3×) 2.216(3×)	2.229(2×) 2.205(2×) 2.228(2×)	2.239, 2.246 2.210(2×) 2.240, 2.247	2.217, 2.218 2.245, 2.243 2.243, 2.251	2.224(2×) 2.241, 2.238 2.219, 2.241
C—O	1.187 1.184 1.193	1.188(3×)	1.183(2×) 1.186	1.186(2×) 1.184	1.189 1.186 1.188	1.183 1.187 1.189
Angle [deg]						
Co—Co—Co	60.1 58.4 61.5	60.0(3×)	61.0 57.9 61.0	59.4 60.9 59.7	60.8 59.6 59.5	61.0 59.4 59.6
$Co—C_{C=O}—Co$	82.3 79.0 80.4	78.9(3×)	78.9(2×) 77.0	81.6 80.4 82.1	79.1(2×) 79.9	80.3 82.4 81.6
$Co—C_{C=O}—O$	158.0/119.6 129.6/151.3 138.1/141.5	140.4(3×)/ 140.7(3×)	137.3/143.8 143.9/137.2 141.5(2×)	133.8/144.5 133.2/146.4 131.9/146.0	141.4/139.5 140.3/139.8 140.5/140.4	131.8, 147.8 132.0, 145.5 135.1, 143.3
P—Co—P	103.4 102.5 100.4	100.1(3×)	100.7(2×) 103.2	98.1 99.4 98.9	100.1 98.5 96.5	98.8 98.0 99.7

Tab. 5. Distances to Co atoms and heights over the Co_3 plane of the H atom in the central μ_3-bridge, H_{centr}, and in the added H_2 unit, H_{H2}, of the model systems $[H_n\{Co(\mu_2\text{-}CO)(PMe_3)_2\}_3]$ in the most stable spin states, M_S.

n	1	2	2	3	4
Model	B	C1	C2	D	E
M_S	3	2	2	3	2
Distance [Å]					
$Co—H_{centr}$	1.693(3×)	1.747/1.739 1.703(2×) 1.738/1.747	–	1.691 1.682 1.694	–
$Co—H_{H2}$	–	–	2.769/3.468 3.504/4.163 2.970/3.623	3.546/4.219 2.960/3.620 3.027/3.736	2.040/3.695, 5.598/6.084 2.815/3.522, 7.095/7.627 3.623/4.275, 5.866/6.533
$(H—H)_{H2}$	–	–	0.746	0.747	0.746, 0.744
Height [Å]					
$Co_3—H_{centr}$	0.955	1.007/1.008	–	0.932	–
$Co_3—H_{H2}$	–	–	2.550/3.278	2.723/3.447	2.613/3.342, 4.546/5.046

Tab. 6. Charges and spin populations of relevant atoms of the model systems $[H_n\{Co(\mu_2\text{-}CO)(PMe_3)_2\}_3]$ in the most stable spin states, M_S.

n	0	1	2	2	3	4
Model	A	B	C1	C2	D	E
M_S	4	3	2	2	3	2
Charge						
Co	0.27 0.46 0.31	0.39(3×)	0.46(2×) 0.40	0.35 0.31 0.33	0.39 0.40 0.41	0.30 0.34(2×)
$C_{C=O}$	0.59(2×) 0.63	0.63(2×) 0.64	0.66 0.69 0.68	0.64 0.63(2×)	0.64(3×)	0.62 0.64 0.63
O	–1.19(2×) –1.18	–1.19(3×)	–1.18(3×)	–1.18 –1.19(2×)	–1.19(2×) –1.18	–1.19(2×) –1.18
P	1.61, 1.54 1.60, 1.55 1.62, 1.60	1.61(3×) 1.59(3×)	1.59(4×) 1.60(2×)	1.58/1.56 1.58/1.59 1.55/1.57	1.59, 1.56 1.58, 1.59 1.62, 1.59	1.56(3×)/ 1.58(3×)
H_{centr}	–	–0.32	–0.29(2×)	–	–0.32	-
H_{H2}	–	–		0.02, –0.06	0.03, –0.06	0.02, –0.05 0.00, –0.00
Spin						
Co	0.70 1.75 0.93	0.80(3×)	0.81(2×) –0.48	1.07 –0.91 0.99	0.78 0.82 0.84	–0.91 1.00 1.05
$C_{C=O}$	–0.10(2×) –0.09	–0.09(3×)	–0.09 –0.00(2×)	–0.08 0.02 –0.04	–0.09(3×)	0.02 –0.04 –0.08
O	–0.07(2×) –0.03	–0.06(3×)	–0.06 –0.00(2×)	–0.06 0.01 –0.03	–0.06(3×)	0.01 –0.03 –0.05
P	0.01(3×) 0.00(3×)	–0.00(4×) 0.01(2×)	0.01(4×) –0.01/–0.00	0.00(6×)	0.01(3×) –0.03(3×)	0.00(5×) 0.01
H_{centr}	–	–0.03	–0.02(2×)	–	–0.03	–
H_{H2}	–	–	–	0.00, 0.01	–0.00, –0.01	0.00(4×)

index for atoms A and B connected by a bond path. Ring critical points (RCP) are located inside cyclic structures with two positive and one negative eigenvalues of the Hessian of RCP electron density. Local minima of electron density are known as cage critical points (CCP) with three positive eigenvalues of the Hessian of CCP electron density.

QTAIM topological analysis of electron density was performed using the AIMAll software (Keith, 2019). The AIM2000 software (Biegler-König et al., 2001) was used to draw molecular graphs of the studied systems. The MOLDRAW software was used for geometry manipulation and visualization (Ugliengo, 2012).

Results and Discussion

Geometry optimization of neutral triangulo-complexes $[\{Co(\mu_2\text{-}CO)(PMe_3)_2\}_3]$ (model A), $[(\mu_3\text{-}H)\{Co(\mu_2\text{-}CO)(PMe_3)_2\}_3]$ (model B), $[(\mu_3\text{-}H)_2\{(\mu_2\text{-}CO)(PMe_3)_2\}_3]$ (model C1), $[(H_2)\{C_3(\mu_2\text{-}CO)(PMe_3)_2\}_3]$ (model C2), $[(H_2)(\mu_3\text{-}H)\{Co(\mu_2\text{-}CO)(PMe_3)_2\}_3]$ (model D), and $[(H_2)_2\{Co(\mu_2\text{-}CO)(PMe_3)_2\}_3]$ (model E) was performed in three lowest spin states (M_S) starting from X-ray structures of $[H_n\{Co(\mu_2\text{-}CO)(PMe_3)_2\}_3]$ and/or their modifications (Klein et al., 1992a; Klein et al., 1997). Starting positions of H_2 molecules in models C2, D, and E were approximately 1.5/2.5 Å over

Tab 7. Delocalization indices, DI, and electron density at bond critical points, ρ_{BCP}, of the relevant bonds of the model systems $[H_n\{Co(\mu_2\text{-}CO)(PMe_3)_2\}_3]$ in the most stable spin states, M_S.

n	0	1	2	2	3	4
Model	A	B	C1	C2	D	E
Ms	4	3	2	2	3	2
DI						
Co—$C_{C=O}$	0.868/0.764 1.130/0.525 0.506/1.073	0.812(3×) 0.779(3×)	0.773/0.728 0.667/0.807 0.810/0.664	1.040/0.545 0.576/1.029 0.538/1.064	0.785/0.772 0.817/0.804 0.798/0.778	1.033/0.594 0.521/1.068 0.549/1.033
Co—P	0.780/0.792 0.671/0.667 0.740/0.737	0.745(3×)	0.723(2×) 0.753(2×) 0.726/0.722	0.705/0.733 0.762/0.767 0.738/0.713	0.743(2×) 0.719/0.717 0.706/0.714	0.761/0.746 0.710/0.734 0.748/0.722
C—O	1.409 1.428 1.434	1.430(3×)	1.445 1.450(2×)	1.451 1.439(2×)	1.433 1.427 1.442	1.432 1.452 1.442
Co—H_{centr}	–	0.366(3×)	0.325/0.332 0.377(2×) 0.324/0.326		0.366 0.375 0.362	–
$(H—H)_{H2}$	–		–	0.876	0.876	0.881 0.974
ρ_{BCP} [e/Bohr^3]						
Co—$C_{C=O}$	0.155, 0.089 0.076, 0.151 0.115, 0.127	0.116(3×) 0.121(3×)	0.118(2×) 0.102/0.121 0.122/0.102	0.144/0.086 0.144/0.148 0.080(2×)	0.122, 0.116 0.118, 0.115 0.119, 0.117	0.144/0.088 0.076/0.149 0.082/0.144
Co—P	0.096(2×) 0.079(2×) 0.089(2×)	0.089(6×)	0.086(2×) 0.091(2×) 0.086(2×)	0.083(2×) 0.090/0.089 0.083(2×)	0.089, 0.088 0.084, 0.083 0.082, 0.084	0.087(3×) 0.084(3×)
C—O	0.423 0.426 0.417	0.421(3×)	0.423 0.426(2×)	0.425 0.422(2×)	0.421 0.423 0.422	0.421 0.427 0.423
Co—H_{centr}	–	0.084(3×)	0.076(2×) 0.085(2×) 0.077(2×)	–	0.084 0.085 0.083	–
$(H—H)_{H2}$	–	–		0.263	0.264	0.262(2×)

the center of the Co_3 triangle. Energy data of optimized structures are presented in Tab. 2. Relative abundances of individual spin states of the same compound (Table 2) were evaluated using Boltzmann statistics. The most stable structures of the remaining models correspond to doublet or triplet spin states, except for model A (the most stable quartet spin state). Structures in the most stable spin states are presented in Fig. 2.

Reaction Gibbs energies of $[\{Co(\mu_2\text{-}CO)(PMe_3)_2\}_3]$ (model A) hydrogenation at various temperatures are presented in Tab. 3 (based on Tab. A1 data in Appendix). It is evident that hydrogenation to models B, C1, and D containing μ_3-H bridges is energetically more advantageous at low temperatures, whereas formation of C2 and E containing only H_2 units is not favored.

Only $[(\mu_3\text{-}H)\{Co\ (\mu_2\text{-}CO)(PMe_3)_2\}_3]$ (model B) in the triplet spin state exhibits trigonal symmetry (see Tab. 4). The lower symmetry of the remaining model systems can be explained by the Jahn-Teller effect and, to a lesser extent, by the non-symmetric location of the H_2 unit. Co—C_{C-O} bond length alternation can be observed in our systems. It can be concluded that μ_3-H bridges stabilize the Co_3 unit (lower average Co—Co distances; see Tab. A2 in Appendix).

Except for the distances Co—Co and Co—$C_{C=O}$ in $[(\mu_3\text{-}H)\{Co(\mu_2\text{-}CO)(PMe_3)_2\}_3]$ (model B) and Co—H_{centr} in $[(H_2)(\mu_3\text{-}H)\{Co(\mu_2\text{-}CO)(PMe_3)_2\}_3]$ (model D), the calculated interatomic distances

Tab. 8. Laplacians ($\nabla^2\rho_{BCP}$) and ellipticities (ε_{BCP}) at bond critical points of the relevant bonds of model systems $[H_n\{Co(\mu_2\text{-}CO)(PMe_3)_2\}_3]$ in the most stable spin states (M_S).

n	0	1	2	2	3	4
Model	A	B	C1	C2	D	E
M_S	4	3	2	2	3	2
$\nabla^2\rho_{BCP}$ [e/Bohr^5]						
Co—$C_{C=O}$	0.342, 0.484 0.189, 0.199 0.293, 0.442	0.319(3×) 0.310(3×)	0.308(2×) 0.250/0.335 0.336/0.249	0.385/0.232 0.369/0.391 0.204/0.211	0.311, 0.322 0.303, 0.311 0.314, 0.304	0.362/0.237 0.198/0.401 0.215/0.382
Co—P	0.195, 0.189 0.197, 0.185 0.199, 0.200	0.205(3×) 0.208(3×)	0.208/0.206 0.202(2×) 0.207(2×)	0.195/0.207 0.204/0.209 0.206/0.199	0.207, 0.203 0.200(2×) 0.198, 0.202	0.205/0.200 0.196/0.208 0.206(2×)
C—O	0.165 0.178 0.204	0.207(3×)	0.230 0.243(2×)	0.230 0.210(2×)	0.214 0.204 0.225	0.201 0.235 0.212
Co—H_{centr}	–	0.201(3×)	0.164/0.166 0.149(2×) 0.165(2×)	–	0.200 0.206 0.204	–
$(H—H)_{H2}$	–	–	–	–1.056	–1.060	–1.058(2×)
ε_{BCP}						
Co—$C_{C=O}$	0.033, 0.032 0.171, 0.123 0.053, 0.006	0.050(3×) 0.056(3×)	0.062(2×) 0.052/0.037 0.036/0.053	0.024/0.155 0.023/0.009 0.181/0.161	0.046, 0.044 0.059, 0.052 0.050, 0.057	0.010/0.175 0.194/0.017 0.131/0.025
Co—P	0.046, 0.198 0.060, 0.097 0.048, 0.069	0.028(3×) 0.034(3×)	0.019/0.036 0.032(2×) 0.036/0.019	0.116/0.056 0.055/0.024 0.051/0.048	0.062, 0.031 0.031, 0.054 0.036, 0.067	0.043/0.028 0.085/0.055 0.071/0.041
C—O	0.038 0.024(2×)	0.037(3×)	0.042 0.038(2×)	0.031(2×) 0.033	0.037 0.035(2×)	0.033(2×) 0.029
Co—H_{centr}	–	0.003(3×)	0.075/0.065 0.003/0.002 0.065/0.074	–	0.031 0.018 0.033	–
$(H—H)_{H2}$	–	–	–	0.000	0.001	0.000(2×)

are longer than their X-ray counterparts (compare Tabs. 1, 4, 5, and A3 in Appendix). The calculated distances between Co atoms and the added H_2 units are too long for any bonding. The Co—$C_{C=O}$—O angles are more variable than other relevant bond angles in the systems under study.

The relevant parts of the QTAIM molecular graphs (Bader, 1994) of the studied model systems are presented in Figs. A1—A6 in Appendix. There are no Co—Co bond paths, which excludes any Co—Co bonding. The same holds for the bond paths between Co atoms and H_2 units. According to the molecular graphs, Co_3 units are held together exclusively by μ_2-CO and μ_3-H bridges. There are bond paths between the H_2 units and methyl atoms that might not be real bonds.

Positive Co charges increase slightly due to μ_3-H presence. Atomic charges of Co (ca +0.3), carbonyl C (ca +0.6), O (ca –1.2) nd P (ca +1.6) do not depend on the number of H atoms added (Tabs. 6 and A4 in Appendix). The charges of the bridging μ_3-H atoms are negative (ca –0.3) unlike the neutral H_2 units. Spin populations (in Tabs. 6 and A4 in Appendix presented as populations of unpaired α or β electrons) are concentrated dominantly at Co atoms. Spin populations at carbonyl groups (prevailingly β electrons) are more than one order lower. The remaining atoms (including μ_3-H atoms) have only a vanishing spin density.

Bond strengths within QTAIM treatment can be deduced from delocalization indices and BCP electron densities that exhibit similar trends (Tabs. 7 and A5 in Appendix). As mentioned above, there is no Co—Co bonding in our systems. Co—$C_{C=O}$ bonds can be divided into two groups according to the alternating Co—$C_{C=O}$ distances. Their

variations can be ascribed mainly to the symmetry decrease due to Jahn-Teller effect despite the stabilizing effect of the H_{centr}—Co bonds. Co—P and much stronger C—O bonds exhibit significantly lower variations. The H_{centr}—Co bonds are not so weak as expected. The H—H bonding in the H_2 unit corresponds to a single bond and is not bonded to the central Co_3 unit.

Except for H_2 units, BCP Laplacians ($\nabla^2\rho_{BCP}$) are positive (Tabs. 8 and A6 in Appendix), which reflects the polarity of the Co—$C_{C=O}$, Co—P, C—O and Co—H_{centr} bonds. Only some Co—$C_{C=O}$ BCP Laplacians significantly deviate from 0.2 e/Bohr^5. Values of $\nabla^2\rho_{BCP}$ of individual bonds in the A model complex differ from the remaining complexes, but no systematic dependence on the hydrogen content has been observed.

In most cases, BCP ellipticity values are small (Tabs. 8 and A6 in Appendix), indicating vanishing mechanical strain in cyclic structures. The only exceptions are some Co—$C_{C=O}$ bonds in the A, C2, and D complexes and one Co—P bond in the C2 complex.

Conclusions

Our results indicate that the most stable A complex is in the quartet spin state whereas the remaining complexes are most stable in their doublet or triplet spin states. Non-vanishing content of other spin states at room temperature is predicted in the A (doublet) and B (singlet) complexes. Pure DFT functionals usually over-stabilize low-spin (LS) states whereas high-spin (HS) states are strongly favored at the Hartree-Fock theory level (Harvey, 2004; Radon, 2019; Ashley and Jakubikova, 2017). In hybrid DFT functionals, the LS-HS energy difference depends on the exact exchange almost linearly with an optimum at ca 15 %; therefore, the B3LYP hybrid functional with 20 % exact exchange provides ground states very close to the experiment. Hydrogenation of the A complex to complexes with μ_3-H bridges (B, C1, and D models) is more advantageous at lower temperatures; formation of complexes without these bridges (C2 and E models) is improbable even at 100 K. The thermal movement explains why X-ray studies of the complexes at room temperature (Klein et al., 1992a) were not successful in locating added hydrogen atoms.

Unlike X-ray studies (Klein et al., 1992a, 1997), trigonal symmetry is preserved only in the B complex. Deviations from this symmetry are probably caused by the Jahn-Teller effect. Nevertheless, dynamical averaging at high temperatures shows the averaged trigonal structures to oppose the experimentally observed ones.

Spin density is concentrated dominantly at positively charged Co atoms whereas only vanishing spin density is located at the negatively charged μ_3-H atoms. This is in contradiction with the assumption of Boča et al. (Boča et al., 2000) in evaluating magnetic measurements. Neutral H_2 units in C2, D, and E complexes have only vanishing spin density.

Results of QTAIM analysis show missing Co—Co bonds and thus the Co_3 triangles are held together only by μ_2-CO and μ_3-H bridges. Missing bonding between positively charged metal atoms is not exceptional in this type of complexes (see e.g. Breza and Biskupic, 2004a, 2004b; Breza and Manova, 2006; Racioppi et al., 2018; Hamza and Al-Ibadi, 2023). The H_2 units in C2, D, and E complexes are only physisorbed. They are located far from the central part of these complexes and their locations should be variable in real systems. Therefore, they are only hardly observed by X-ray experiments.

Finally, it can be concluded that the X-ray experiments of $[H_n\{Co(\mu_2\text{-}CO)(PMe_3)_2\}_3]$ complexes should be performed at low temperatures and magnetic measurements should be interpreted in terms of the Co—Co interactions only.

Acknowledgement

This research has been supported by the Slovak Scientific Grant Agency VEGA (projects nos. 1/0175/23 and 1/0324/24). The author thanks the HPC center at the Slovak University of Technology in Bratislava, which is a part of the Slovak Infrastructure of High-Performance Computing (SIVVP project ITMS 26230120002, funded by European Region Development Funds) for computational time and resources made available.

References

Ashley DC, Jakubikova E (2017) Coord. Chem. Rev. 337: 97—111.

Bader RFW (1994) Atoms in Molecules. A Quantum Theory. Oxford University Press, Oxford.

Becke AD (1993) J. Chem. Phys. 98: 5648—5652.

Biegler-König F, Schönbohm J, Bayles D (2001) J. Comput. Chem. 22: 545—559.

Boča R, Klein H-F, Schmidt A, Valko M, Linert W (2000) Chem. Phys. Lett. 323: 243—248.

Böhme DK, Schwarz H (2005) Angew. Chem. Int. Ed. 44(16): 2336—2354.

Bradamante P, Pino P, Stefani A, Facchinetti G, Zanazzi PF (1983) J. Organomet. Chem. 251: C47—C49.

Breza M (1994) Polyhedron 13(1): 105—107.

Breza M, Biskupic S (2004a) Coll. Czech. Chem. Commun. 69(11): 2045—2054.

Breza M, Biskupic S (2004b) Coll. Czech. Chem. Commun. 69(11): 2055—2067.

Breza M, Manova A (2006) J. Mol. Struct. (THEOCHEM) 765(1-3): 121—126.

Craig GA, Murrie M (2015) Chem. Soc. Rev. 44(8): 2135—2147.

Facchinetti G, Pucci S, Zanazzi PF, Methong U (1979) Angew. Chem., Int. Ed. Engl. 18: 619—620.
Facchinetti G, Balocchi L, Secco F, Venturini M (1981) Angew. Chem., Int. Ed. Engl. 20: 204—205.
Frisch MJ, Trucks GW, Schlegel HB, Scuseria GE, Robb MA, Cheeseman JR, Scalmani G, Barone V, Petersson GA, Nakatsuji H, Li X, Caricato M, Marenich AV, Bloino J, Janesko BG, Gomperts R, Mennucci B, Hratchian HP, Ortiz JV, Izmaylov AF, Sonnenberg JL, Williams-Young D, Ding F, Lipparini F, Egidi F, Goings J, Peng B, Petrone A, Henderson T, Ranasinghe D, Zakrzewski VG, Gao J, Rega N, Zheng G, Liang W, Hada M, Ehara M, Toyota K, Fukuda R, Hasegawa J, Ishida M, Nakajima T, Honda Y, Kitao O, Nakai H, Vreven T, Throssell K, Montgomery JA Jr, Peralta JE, Ogliaro F, Bearpark MJ, Heyd JJ, Brothers EN, Kudin KN, Staroverov VN, Keith TA, Kobayashi R, Normand J, Raghavachari K, Rendell AP, Burant JC, Iyengar SS, Tomasi J, Cossi M, Millam JM, Klene M, Adamo C, Cammi R, Ochterski JW, Martin RL, Morokuma K, Farkas O, Foresman JB, Fox DJ (2016) Gaussian 16, Rev C01, Gaussian, Inc., Wallingford, CT.
Grimme S, Antony J, Ehrlich S, Krieg H (2010) J. Chem. Phys. 132: 154104
Guzman-Jimenez IY, van Hal JW, Whitmire KH (2003) Organometallics 22(9): 1914—1922.
Hamza NA, Al-Ibadi MAM (2023) Theor. Chem. Accounts 142(11): 00120.
Harvey N (2004) Struct. Bonding 112: 151—183.
Hogarth G, Kabir SE, Nordlander E (2010) Dalton Trans. 39(27): 6153—6174.
Keith TA (2019) AIMAll (Version 19.10.12). TK Gristmill Software, Overland Park, KS, USA (http://aim.tkgristmill.com).
Klein H-F, Mager M, Florke U, Haupt H-J, Breza M, Boca R (1992a) Organometallics 11: 2912—2916.
Klein H-F, Mager M, Isringhausen-Bley S, Florke U, Haupt H-J (1992b) Organometallics 11(10): 3174—3175.
Klein H-F, Mager M, Schmidt A, Huber M, Haase W, Florke U, Haupt H-J, Boca R (1997) Inorg. Chem. 36: 4303—4306.
Liu K, Shi W, Cheng P (2015) Coord. Chem. Rev. 289: 74—122.
Malrieu J-P, Trinquier G (2012) J. Phys. Chem. A 116: 8226—8237.
Moberg V, Homanen P, Selva S, Persson R, Haukka M, Pakkanen TA, Monari M, Nordlander E (2006) Dalton Trans. 279—288.
Nombel P, Lugan N, Donnadieu B, Lavigne G (1999) Organometallics 18(2): 187—196.
Pregaglia GF, Andreetta A, Ferrari GF, Ugo R (1969) J. Chem. Soc. D 590—591.
Racioppi S, Della Pergola R, Colombo V, Sironi A, Macchi P (2018) J. Phys. Chem. 122(22): 5004—5015.
Radon M (2019) Adv. Inorg. Chem. 73: 221—264.
Saito T, Kataoka Y, Nakanishi Y, Matsui T, Kitagawa Y, Kawakami T, Okumura M, Yamaguchi K (2009) Int. J. Quantum Chem. 109: 3649—3658.
Tsukamoto T (2024) Nanoscale 16: 10533.
Ugliengo P (2012) MOLDRAW: A Program to Display and Manipulate Molecular and Crystal Structures, University Torino, Torino. Available online: https://moldraw.software.informer.com (accessed on 9 September 2019).

Appendix

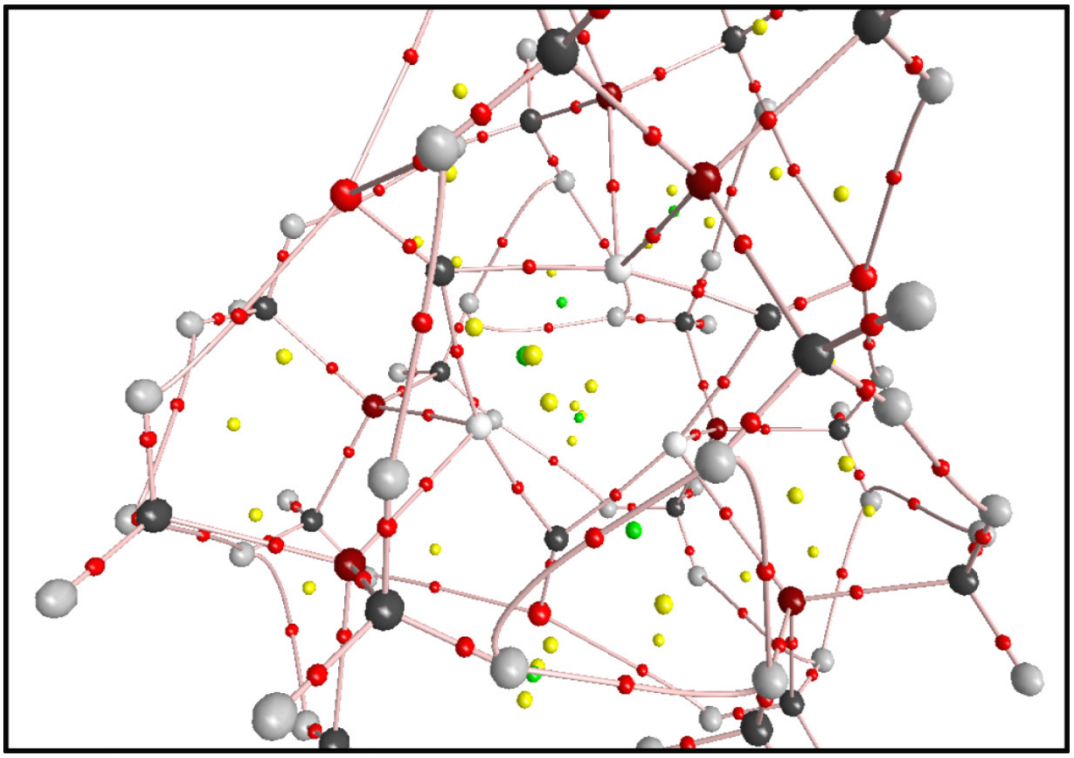

Fig. A1. Relevant parts of molecular graph of $^{4}[\{Co(\mu_2\text{-}CO)(PMe_3)_2\}_3]^0$, model A (Co – light gray, C – black, O – big red, P – dark red, H – dark gray, bond critical points – small red, ring critical points – yellow, cage critical points – green).

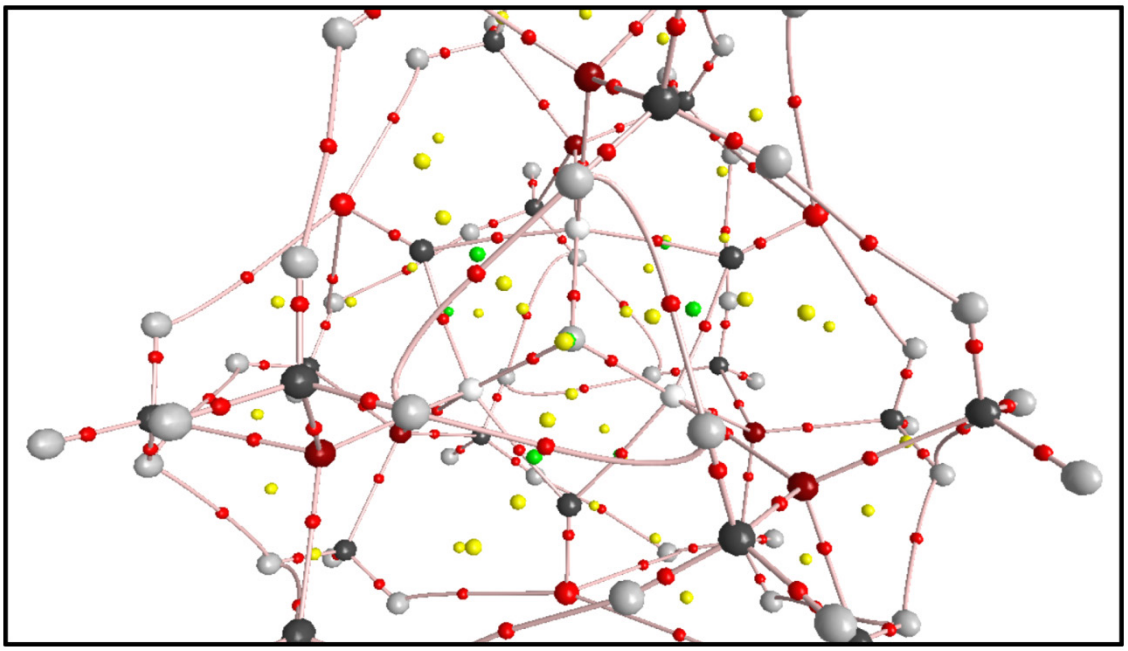

Fig. A2. Relevant parts of molecular graph of $^{3}[(\mu_3\text{-}H)\{Co(\mu_2\text{-}CO)(PMe_3)_2\}_3]^0$, model B (Co – light gray, C – black, O – big red, P – dark red, H – dark gray, bond critical points – small red, ring critical points – yellow, cage critical points – green).

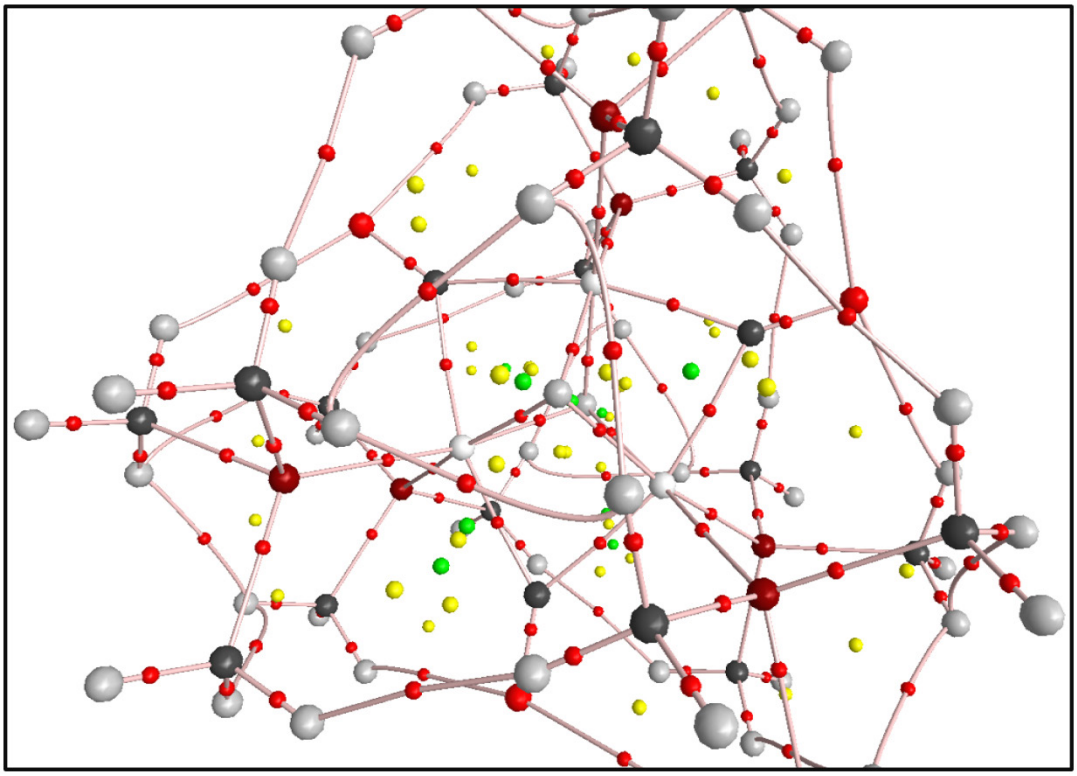

Fig. A3. Relevant parts of molecular graph of $^{2}[(\mu_3\text{-H})_2\{Co(\mu_2\text{-CO})(PMe_3)_2\}_3]^0$, model C1 (Co — light gray, C — black, O — big red, P — dark red, H — dark gray, bond critical points — small red, ring critical points — yellow, cage critical points — green).

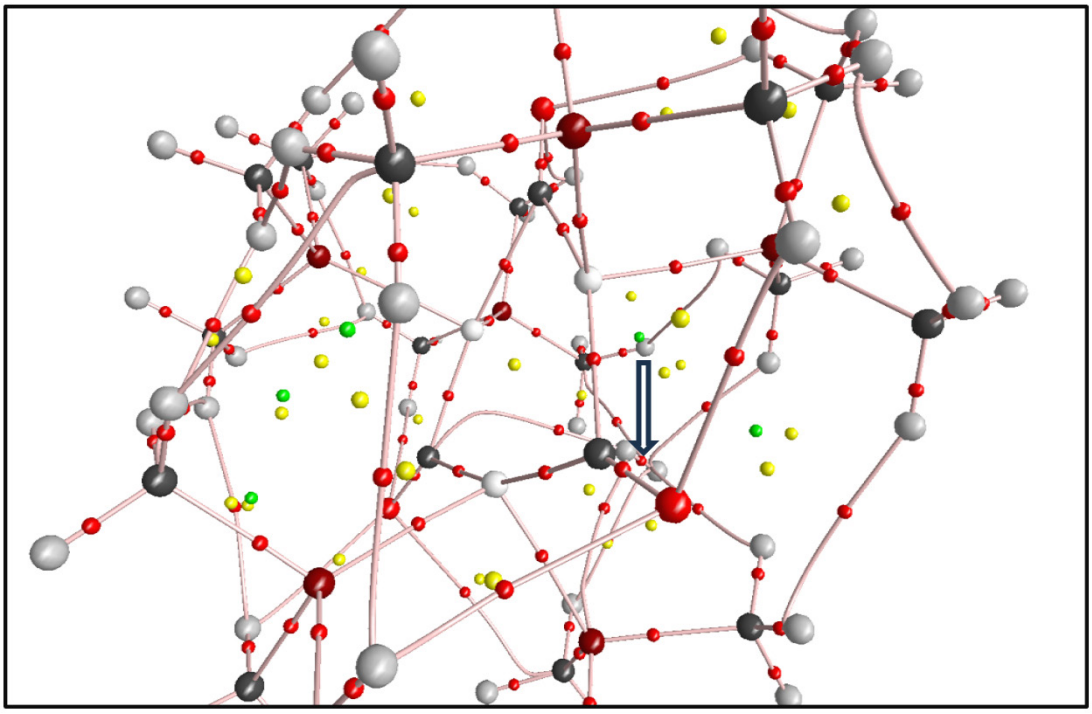

Fig. A4. Relevant parts of molecular graph of $^{2}[H_2\{Co(\mu_2\text{-CO})(PMe_3)_2\}_3]^0$, model C2 (Co — light gray, C — black, O — big red, P — dark red, H — dark gray, bond critical points — small red, ring critical points — yellow, cage critical points — green). Arrow denotes the H_2 molecule.

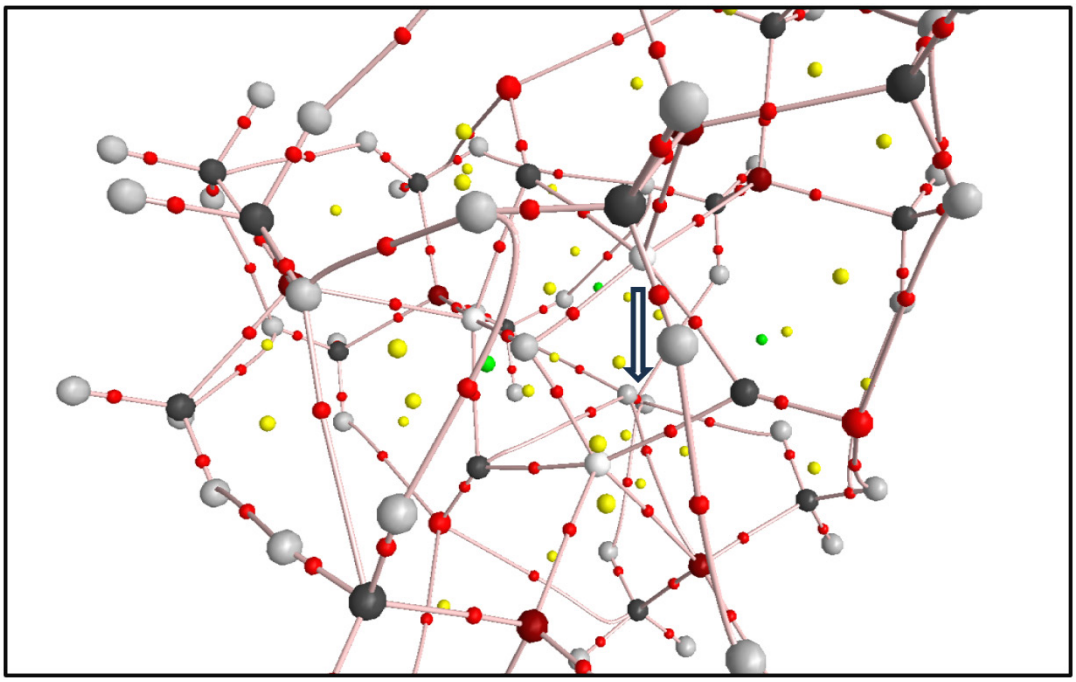

Fig. S5. Relevant parts of molecular graph of $^{3}[(\mu_3\text{-H})H_2\{Co(\mu_2\text{-CO})(PMe_3)_2\}_3]^0$, model D (Co – light gray, C – black, O – big red, P – dark red, H – dark gray, bond critical points – small red, ring critical points – yellow, cage critical points – green). Arrow denotes the H_2 molecule.

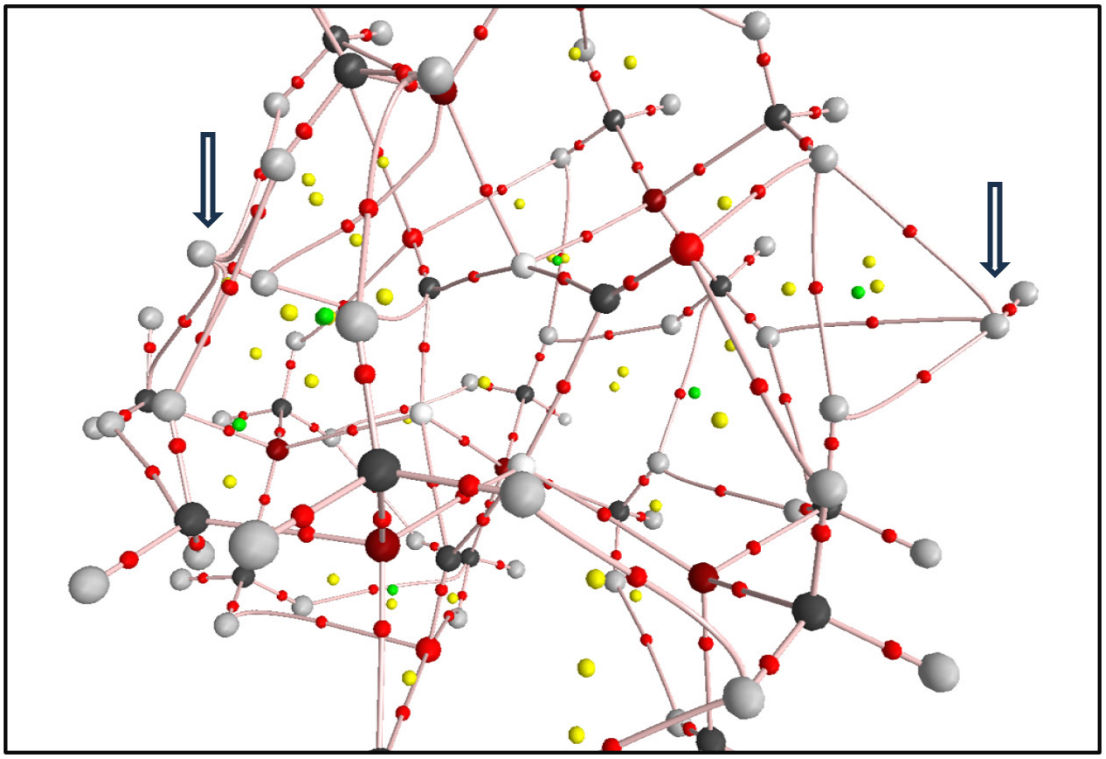

Fig. A6. Relevant parts of molecular graph of $^{2}[(H_2)_2\{Co(\mu_2\text{-CO})(PMe_3)_2\}_3]^0$, model E (Co – light gray, C – black, O – big red, P – dark red, H – dark gray, bond critical points – small red, ring critical points – yellow, cage critical points – green). H_2 molecules are denoted by arrows.

Tab. A1. Gibbs energies (G_T) calculated at various absolute temperatures (T).

Model	Molecule	G_{298} [Hartree]	G_{200} [Hartree]	G_{100} [Hartree]
A	$^4[\{Co(\mu_2\text{-}CO)(PMe_3)_2\}_3]^0$	–7254.94657	–7254.90356	–7254.87262
B	$^3[(\mu_3\text{-}H)\{Co(\mu_2\text{-}CO)(PMe_3)_2\}_3]^0$	–7255.55797	–7255.51631	–7255.48666
C1	$^2[(\mu_3\text{-}H)_2\{Co(\mu_2\text{-}CO)(PMe_3)_2\}_3]^0$	–7256.12844	–7256.08610	–7256.05600
C2	$^2[(H_2)\{Co(\mu_2\text{-}CO)(PMe_3)_2\}_3]^0$	–7256.09832	–7256.05559	–7256.02515
D	$^3[(H_2)(\mu_3\text{-}H)\{Co(\mu_2\text{-}CO)(PMe_3)_2\}_3]^0$	–7256.71265	–7256.67009	–7256.63982
E	$^2[(H_2)_2\{Co(\mu_2\text{-}CO)(PMe_3)_2\}_3]^0$	–7257.27248	–7257.22734	–7257.19619
–	$^1(H_2)^0$	–1.18100	–1.17633	–1.17215

Tab. A2. Averaged relevant interatomic distances and bond angles in model systems $[H_n\{Co(\mu_2\text{-}CO)(PMe_3)_2\}_3]$ in the most stable spin states (M_S).

n	0	1	2	2	3	4
Model	A	B	C1	C2	D	E
M_S	4	3	2	2	3	2
Distance [Å]						
Co—Co	2.486	2.420	2.433	2.545	2.439	2.546
Co—$C_{C=O}$	1.917	1.904	1.927	1.946	1.909	1.946
Co—P	2.225	2.215	2.221	2.232	2.236	2.231
C—O	1.188	1.188	1.184	1.185	1.188	1.186

Tab. A3. Averaged distances to Co atoms and heights over the Co_3 plane of the H atom in the central μ_3-bridge (H_{centr}), and in the added H_2 unit (H_{H2}) of model systems $[H_n\{Co(\mu_2\text{-}CO)(PMe_3)_2\}_3]$ in the most stable spin states (M_S).

n	1	2	2	3	4
Model	B	C1	C2	D	E
M_S	3	2	2	3	2
Distance [Å]					
Co—H_{centr}	1.693	1.730	–	1.689	–
Co—H_{H2}	–	–	3.416	3.518	3.328, 6.467
$(H—H)_{H2}$	–	–	0.746	0.747	0.745
Height [Å]					
Co_3—H_{centr}	0.955	1.007	–	0.932	–
Co_3—H_{H2}	–	–	2.550/3.278	2.723/3.447	2.613/3.342, 4.546/5.046

Tab. A4. Averaged charges and spin populations of relevant atoms of model systems $[H_n\{Co(\mu_2\text{-}CO)(PMe_3)_2\}_3]$ in the most stable spin states (M_S).

n	0	1	2	2	3	4
Model	A	B	C1	C2	D	E
M_S	4	3	2	2	3	2
Charge						
Co	0.35	0.39	0.42	0.33	0.40	0.31
$C_{C=O}$	0.61	0.63	0.67	0.63	0.64	0.63
O	–1.19	–1.19	–1.18	–1.19	–1.19	–1.19
P	1.59	1.60	1.59	1.57	1.59	1.57
H_{centr}	–	–0.32	–0.29	–	–0.32	–
H_{H2}	–	–		–0.04	–0.03	–0.03 0.00
Spin						
Co	1.13	0.80	0.38	0.38	0.81	0.38
$C_{C=O}$	–0.10	–0.09	–0.03	–0.03	–0.09	–0.03
O	–0.06	–0.06	–0.02	–0.03	–0.06	–0.02
P	0.01	–0.00	0.01	0.00	–0.01	0.00
H_{centr}	–	–0.03	–0.02	–	–0.03	–
H_{H2}	–	–	–	0.00	–0.00	0.00

Tab. A5. Averaged delocalization indices (DI), and electron density at bond critical points (ρ_{BCP}), of relevant bonds of model systems $[H_n\{Co(\mu_2\text{-}CO)(PMe_3)_2\}_3]$ in the most stable spin states (M_S).

n	0	1	2	2	3	4
Model	A	B	C1	C2	D	E
M_S	4	3	2	2	3	2
DI						
Co—$C_{C=O}$	0.811	0.796	0.742	0.799	0.792	0.800
Co—P	0.731	0.745	0.733	0.736	0.724	0.737
C—O	1.424	1.430	1.448	1.443	1.434	1.442
Co—H_{centr}	–	0.366	0.344		0.368	–
$(H—H)_{H2}$	–		–	0.876	0.876	0.881 0.974
ρ_{BCP} [e/Bohr^3]						
Co—$C_{C=O}$	0.119	0.119	0.114	0.114	0.118	0.114
Co—P	0.088	0.089	0.088	0.085	0.085	0.085
C—O	0.422	0.421	0.425	0.423	0.422	0.424
Co—H_{centr}	–	0.084	0.079	–	0.084	
Co—H_{H2}	–	–	–		–	
$(H—H)_{H2}$	–	–		0.263	0.264	0.262(2×)

Tab. A6. Averaged Laplacians ($\nabla^2\rho_{BCP}$), and ellipticities (ε_{BCP}) at bond critical points of relevant bonds of model systems $[H_n\{Co(\mu_2\text{-}CO)(PMe_3)_2\}_3]$ in the most stable spin states (M_S).

n	0	1	2	2	3	4
Model	A	B	C1	C2	D	E
M_S	4	3	2	2	3	2
$\nabla^2\rho_{BCP}$ [e/Bohr^5]						
Co—$C_{C=O}$	0.325	0.315	0.298	0.299	0.311	0.299
Co—P	0.194	0.207	0.205	0.203	0.203	0.206
C—O	0.182	0.207	0.234	0.216	0.214	0.216
Co—H_{centr}	–	0.201	0.160	–	0.203	–
$(H—H)_{H2}$	–	–	–	–1.056	–1.060	–1.058
ε_{BCP}						
Co—$C_{C=O}$	0.084	0.053	0.050	0.092	0.051	0.092
Co—P	0.086	0.033	0.029	0.058	0.047	0.054
C—O	0.031	0.037	0.039	0.032	0.036	0.032
Co—H_{centr}	–	0.003	0.047	–	0.027	–
$(H—H)_{H2}$	–	–	–	0.000	0.001	0.000(2×)